

# BETA DIPS IN THE *GAIA* ERA: SIMULATION PREDICTIONS OF THE GALACTIC VELOCITY ANISOTROPY PARAMETER ( $\beta$ ) FOR STELLAR HALOS

SARAH R. LOEBMAN<sup>1,2</sup>, MONICA VALLURI<sup>1</sup>, KOHEI HATTORI<sup>1</sup>, VICTOR P. DEBATTISTA<sup>3</sup>, ERIC F. BELL<sup>1</sup>, GREG STINSON<sup>4</sup>,  
CHARLOTTE R. CHRISTENSEN<sup>5</sup>, ALYSON BROOKS<sup>6</sup>, THOMAS R. QUINN<sup>7</sup>, AND FABIO GOVERNATO<sup>7</sup>

*Draft version April 24, 2017*

## ABSTRACT

The velocity anisotropy parameter,  $\beta$ , is a measure of the kinematic state of orbits in the stellar halo which holds promise for constraining the merger history of the Milky Way (MW). We determine global trends for  $\beta$  as a function of radius from three suites of simulations, including accretion only and cosmological hydrodynamic simulations. We find that both types of simulations are consistent and predict strong radial anisotropy ( $\langle\beta\rangle\sim 0.7$ ) for Galactocentric radii greater than 10 kpc. Previous observations of  $\beta$  for the MW’s stellar halo claim a detection of an isotropic or tangential “dip” at  $r\sim 20$  kpc. Using the  $N$ -body+SPH simulations, we investigate the temporal persistence, population origin, and severity of “dips” in  $\beta$ . We find dips in the *in situ* stellar halo are long-lived, while dips in the accreted stellar halo are short-lived and tied to the recent accretion of satellite material. We also find that a major merger as early as  $z\sim 1$  can result in a present day low (isotropic to tangential) value of  $\beta$  over a wide range of radii. While all of these mechanisms are plausible drivers for the  $\beta$  dip observed in the MW, in the simulations, each mechanism has a unique metallicity signature associated with it, implying that future spectroscopic surveys could distinguish between them. Since an accurate knowledge of  $\beta(r)$  is required for measuring the mass of the MW halo, we note significant transient dips in  $\beta$  could cause an overestimate of the halo’s mass when using spherical Jeans equation modeling.

**Keywords:** Galaxy: formation — Galaxy: evolution — Galaxy: kinematics and dynamics — Galaxy: structure — Galaxy: halo — Galaxy: abundances

## 1. INTRODUCTION

It is widely assumed that the kinematic state of the stellar halo can be used to constrain the Milky Way’s (MW) formation history (Eggen et al. 1962; Johnston et al. 2008) and mass distribution (Xue et al. 2008; Gnedin et al. 2010; Deason et al. 2012). As a result, a considerable effort has been expended in measuring the stellar halo’s kinematic moments (*e.g.*, Xue et al. 2008; Bond et al. 2010; Cunningham et al. 2016). Recently, emphasis has been placed on the measurement of the velocity anisotropy parameter ( $\beta$ ), the ratio of tangential to radial random motion, which is expected to be positive from simple numerical experiments of halo formation (Binney & Tremaine 2008). However measurements of  $\beta$  in the MW have suggested that it is negative within  $15\lesssim R/\text{kpc}\lesssim 25$  (see Kafle et al. 2012, King et al. 2015, but see Deason et al. 2013b, Cunningham et al. 2016 for alternative values), leading to speculation that the exact merger and dissipation history of the stellar halo could strongly affect its velocity anisotropy profile (Deason et al. 2013a,b). In spite of

these recent efforts to infer the MW’s accretion history from measurements of the density profile and  $\beta$ , there have been no systematic studies of how  $\beta$  varies with radius in realistic cosmological hydrodynamic simulations that demonstrate that  $\beta$  is in fact a tracer of assembly history.

First introduced by Binney (1980) to characterize the orbital structure of a spherical system,  $\beta$  is most commonly used in spherical Jeans equation modeling to recover the mass distribution of galactic systems. In a Galactocentric spherical coordinate system ( $r, \theta, \phi$ ), corresponding to radial distance, polar angle, and azimuthal angle, we define  $\beta$  as:

$$\beta(r) = 1 - \frac{\sigma_\theta(r)^2 + \sigma_\phi(r)^2}{2\sigma_r(r)^2}, \quad (1)$$

where  $\sigma_\theta, \sigma_\phi, \sigma_r$  are the velocity dispersions in spherical coordinates. In a system in which  $\beta = 1$ , all stars are on radial orbits plunging in and out of the galactic center, while in a system with  $\beta = -\infty$ , all orbits are circular. A system with an isotropic velocity distribution ( $\sigma_\theta = \sigma_\phi = \sigma_r$ ) has  $\beta = 0$ .

Models of galaxy formation generally imply that  $\beta$  increases with radius, corresponding to nearly isotropic near the center and radially biased in the outskirts (see §4.10.3 of Binney & Tremaine 2008, and references therein; Debattista et al. 2008). This trend has been shown in both cosmological pure  $N$ -body simulations (see Figure 10, Diemand et al. 2005) and in cosmological  $N$ -body+SPH simulations (see Figure 5, Sales et al. 2007; Abadi et al. 2006). Analyzing the  $z = 0$  snapshot of the high resolution MW-like simulation Eris,

<sup>1</sup> Department of Astronomy, University of Michigan, 1085 S. University Ave, Ann Arbor, MI 48109-1107, USA; sloebman@umich.edu

<sup>2</sup> Michigan Society of Fellows

<sup>3</sup> Jeremiah Horrocks Institute, University of Central Lancashire, Preston, PR1 2HE, UK

<sup>4</sup> Max-Planck-Institut für Astronomie, Heidelberg, Germany

<sup>5</sup> Physics Department, Grinnell College, Grinnell, IA, USA

<sup>6</sup> Department of Physics & Astronomy, Rutgers University, New Brunswick, NJ, USA

<sup>7</sup> Astronomy Department, University of Washington, Seattle, WA, USA

Rashkov et al. (2013) also found  $\beta$  to be increasingly radially biased with distance, transitioning to purely radial stellar orbits beyond 100 kpc (see §4 and Figure 2, Rashkov et al. 2013). Notably, Eris shows a “dip” in  $\beta$  at  $r \sim 70$  kpc, where  $\beta$  drops from  $\sim 0.75$  to  $0.5$  over a narrow range of radii, which coincides with recently accreted substructure (see Figure 3, Rashkov et al. 2013). This hints that fluctuations in the value of  $\beta$  are possible in simulations, but does not speak directly to their duration, intensity or frequency of occurrence. Recently, using orbital integration analysis, Bird & Flynn (2015) considered the duration of low values in  $\beta$  and found them to be short lived (persisting a few tens of Myr) and unconnected to the galactic density profile. Motivated by this analysis, we look at the time evolution of  $\beta$  simulated in a full cosmological context, to understand what, if any, predictive power  $\beta$  holds for constraining the formation history of the MW.

From an observational perspective,  $\beta$  is hard to measure and somewhat sensitive to small number statistics. For MW halo stars, the form of the  $\beta$ -profile measured also depends on the modeling method employed. Assuming the MW is well described by a truncated, flat rotation curve, it is possible to derive the velocity anisotropy profile from 4D data (Galactocentric radius, on-sky position and line-of-sight velocity) using an action-based distribution function method (see, for instance, Wilkinson & Evans 1999; Deason et al. 2012). Recently, Williams & Evans (2015) constrained such a model using the blue horizontal branch catalog of Xue et al. (2011). Their best fit result for  $\beta(r)$  rises appreciably more gradually than  $\beta(r)$  from  $N$ -body simulations (see Figure 8 and §5.3 Williams & Evans 2015, for further details).

In contrast, measurements of  $\beta$  for halo stars within the solar cylinder based on full 6D phase space data find  $\beta$  to be strongly radially biased. For example, Chiba & Yoshii (1998) analyzed the kinematics of nearby stars falling within  $\sim 2$  kpc from the Sun. They leveraged proper motion (and parallax for a handful of stars) from *Hipparcos* satellite and the photometric distance, line-of-sight velocity and  $[\text{Fe}/\text{H}]$  from ground-based telescopes. Using 124 stars with  $[\text{Fe}/\text{H}] < -1.6$ , Chiba & Yoshii (1998) found velocity dispersions  $(\sigma_r, \sigma_\phi, \sigma_\theta) \simeq (\sigma_U, \sigma_V, \sigma_W) = (161 \pm 10, 115 \pm 7, 108 \pm 7) \text{ km s}^{-1}$ , corresponding to  $\beta = 0.52 \pm 0.07$ . Sampling a larger volume (within 5 kpc of the Sun), Smith et al. (2009) found  $\beta = 0.69 \pm 0.01$ . This value was determined using a catalog of  $\sim 1700$  halo subdwarfs selected using a reduced proper-motion diagram applied to SDSS Stripe 82 data; and combined with radial velocities from SDSS spectra, and distances from the photometric parallax relation (with uncertainty of  $\sim 10\%$ ), Smith et al. (2009) found  $(\sigma_r, \sigma_\phi, \sigma_\theta) = (143 \pm 2, 82 \pm 2, 77 \pm 2) \text{ km s}^{-1}$ . Sampling a slightly larger footprint still ( $r < 10$  kpc) pointed toward the northern Galactic cap, Bond et al. (2010) found a similar value,  $\beta \sim 0.67$ . This was determined using proper motions of a large sample of main sequence SDSS stars from Munn et al. (2004) resulting in  $(\sigma_r, \sigma_\phi, \sigma_\theta) \sim (141, 85, 75) \text{ km s}^{-1}$ .

Beyond  $r \sim 10$  kpc, it has been extremely difficult to obtain full 6D information for a robust sample of halo stars. Since 2014, the HALO7D project (Cunningham et al. 2015) has worked to obtain accu-

rate HST-measured proper motions and very deep Keck DEIMOS spectroscopy of  $\sim 100$  MW main sequence turn-off stars with the goal of assessing  $\beta$  at large radii. Analysis of 13 HALO7D stars lying within  $18 < r/\text{kpc} < 32$  yields  $\beta = -0.3^{+0.4}_{-0.9}$  (Cunningham et al. 2016). This value is consistent with isotropy and lower than the solar neighborhood  $\beta$  measurements by  $2\sigma$ . This value is also substantially lower than model predictions of radially biased values; however, model predictions in the literature were generated in the limit that there was no satellite substructure present. Cunningham et al. (2016) note that two stars from this sample are likely members of a known substructure (TriAnd). If they exclude these stars from their analysis, they find  $\beta = 0.1^{+0.4}_{-1.0}$ , which is still formally lower than solar neighborhood measurements but just outside the  $1\sigma$  limit.

There is a robust and interesting discussion in the literature of the value of  $\beta$  beyond  $r \sim 20$  kpc based upon 4D phase-space information for thousands of blue horizontal branch stars (Sirko et al. 2004; Deason et al. 2012; Kafle et al. 2012; King et al. 2015) and 5D phase-space for a small number of halo stars (Deason et al. 2013b). Wildly divergent values for  $\beta$  have been obtained; based upon these studies, it is plausible that  $\beta$  remains radially anisotropic (Deason et al. 2012),  $\beta$  “dips”, falling from a radial  $\beta \sim 0.5 - 0.7$  value at  $r < 20$  kpc to an isotropic  $\beta \sim 0$  (Sirko et al. 2004; Deason et al. 2013b) or  $\beta$  is strongly tangentially biased, with  $\beta < -1.5$  (Kafle et al. 2012; King et al. 2015) at  $r \sim 20 - 25$  kpc. Deason et al. (2013b) speculate that this dip could be associated with a large, shell-type structure that is a remnant of an accretion event at  $r \sim 25$  kpc; however, Johnston et al. (2008) find shell-type structures to be typically associated with stars on radial orbits at apogalactic passage.

In a companion paper (Hattori et al. 2017), we consider the impact of using 4D data instead of full 6D data to estimate  $\beta$ . We find  $\beta$  is systematically underestimated beyond a certain radius ( $r \sim 15$  kpc for the currently available sample size). As  $r$  increases, the line-of-sight velocity approaches the Galactocentric radial velocity. This makes it difficult to extract information about the tangential velocity distribution (and hence  $\beta$ ) from the line-of-sight velocity distribution alone. The limitation of the line-of-sight velocities to recover the velocity anisotropy was first explored in Hattori et al. (2013) and is supported by Wang et al. (2015), who find that if proper motions are not available, it is difficult to obtain robust constraints on  $\beta$ . Thus for the remainder of this paper, we will focus on  $\beta$  derived from 6D phase-space information.

In anticipation of *Gaia* filling in the gaps and tightening constraints on  $\beta(r)$  for the MW (Gaia Collaboration et al. 2016), in this paper, we consider what high resolution MW-like simulations predict for  $\beta(r)$ . We aim to assemble a comprehensive set of predictions for  $\beta(r)$  for observers to reference and challenge in the coming years. In §2, we discuss the set-up of the three suites of simulations we use. In §3, we present average trends in  $\beta(r)$ ; we find that all three suites are consistent and predict a monotonically increasing value of  $\beta$  that is radially biased, and beyond 10 kpc,  $\beta > 0.5$ . We also consider  $\beta$  as a function of time for individual simulated galaxies, and discuss when and

why “dips” in  $\beta$  form<sup>8</sup> and the rarity of  $\beta < 0$  values, the origin and persistence of these dips in the *in situ* and accreted halo. We also highlight one simulation that is a  $\beta(r)$  outlier: while this galaxy appears to be a normal MW-like disk galaxy at present day, it experienced a major merger with a gas rich system at  $z \sim 1$ . This event left a lasting imprint on  $\beta(r)$ ; the stellar halo has a persistently tangential  $\beta$  profile over a wide range of radii until the present day. We speculate that if the MW went through a similar cataclysmic event, then the signature in  $\beta(r)$  should be visibly present in the MW’s stellar halo today and measurable in the foreseeable future. If, on the other hand, the dip at  $r \sim 20$  kpc is confirmed or other dips are found, we suggest that these are ideal locations to carry out a follow up search for either substructure or *in situ* halo stars. These two possibilities can be distinguished by the metallicity and  $\alpha$ -abundance patterns of the stars giving rise to the  $\beta$  dip. We discuss these results and draw further conclusions in §4.

## 2. SIMULATIONS

We analyze 3 different suites of high resolution MW-like stellar halo simulations: a hybrid  $N$ -body + semi-analytic suite and two fully  $N$ -body+SPH suites with differing prescriptions for star formation and stellar feedback.

### 2.1. Bullock & Johnston Suite

We consider 11 stellar halos from Bullock & Johnston (2005) (henceforth BJ05) which are modeled using the hybrid  $N$ -body + semi-analytic approach. These models are publicly available<sup>9</sup> and are described in detail in Bullock & Johnston (2005); Robertson et al. (2005); Font et al. (2006).

BJ05 assumes a  $\Lambda$ CDM framework with a  $\Omega_m = 0.3$ ,  $\Omega_\Lambda = 0.7$ ,  $\Omega_b h^2 = 0.024$ ,  $h = 0.7$  cosmology. They generate 11 merger histories for a  $z = 0$ ,  $M_{vir} = 1.4 \times 10^{12} M_\odot$  dark matter halo using the method described in Somerville & Kolatt (1999). For each merger event above  $5 \times 10^6 M_\odot$ , an  $N$ -body simulation of a dark matter satellite disrupting in an analytic, time-dependent galaxy + spherical dark matter halo is modeled. The baryonic component of each satellite is modeled using semi-analytic prescriptions and the star formation is truncated soon after each satellite halo is accreted on to the MW host.

While BJ05 neglect satellite-satellite interactions and lack a responsive “live” halo and central galaxy, their methods have provided robust predictions for the spatial and velocity structure of stellar halos and streams in the outer parts of galaxies ( $\geq 20$  kpc), as well as reasonable estimates for global stellar halo properties from accreted material (mass and time evolution) at all radii (Bell et al. 2008). Moreover, their models sample a wide range of merger histories within allowable bounds for the MW, which makes them valuable for gaining intuition about the effects of mergers on the phase-space distribution of the stellar halo at present day.

### 2.2. *g14 Suite*

We use the *g14* (Christensen et al. 2012) suite of simulations which contains four cosmologically derived (Spergel et al. 2003, WMAP3) MW-mass galaxies evolved to redshift zero using the parallel  $N$ -body+SPH code GASOLINE (Wadsley et al. 2004). These galaxies have a spatial resolution of 170 pc and mass resolutions of  $1.3 \times 10^5$ ,  $2.7 \times 10^4$ , and  $8.0 \times 10^3 M_\odot$  for the dark matter, gas and stars, respectively, while also including the large-scale environment by using the ‘zoom-in’ volume renormalization technique (Katz & White 1993) to create the initial conditions. These simulations use a redshift dependent cosmic UV background and realistic cooling and heating, including cooling from metal lines (Shen et al. 2010). Supernovae feedback is modeled using the “blastwave” approach (Stinson et al. 2006) in which cooling is temporarily disabled based on the local gas characteristics. The probability of star formation is a function of the non-equilibrium  $H_2$  abundances (Christensen et al. 2012). The result of tying the star formation to the molecular hydrogen abundance is a greater concentration of the stellar feedback energy and the more efficient generation of outflows. These outflows ensure that the final galaxies have appropriate rotation curves (Governato et al. 2012), stellar mass fractions (Munshi et al. 2013), and dwarf satellite populations (Zolotov et al. 2012; Brooks & Zolotov 2014).

### 2.3. *MaGICC Suite*

We utilize 2 cosmological hydrodynamic simulations from the Making Galaxies in a Cosmological Context (*MaGICC*, Stinson et al. 2013) suite of simulations. Like the *g14* suite, the *MaGICC* galaxies were generated using GASOLINE (Wadsley et al. 2004); however, instead of disabling cooling at early times, the *MaGICC* implementation includes early stellar feedback from massive stars, which is purely thermal and operates much like an ultraviolet ionization source. The early heating of the gas suppresses a higher fraction of star formation prior to  $z = 1$  than supernovae feedback alone; thus, the *MaGICC* galaxies do not suffer from overcooling, and have smaller central bulges in the MW host galaxies and more realistic stellar content in satellite galaxies.

The *MaGICC* simulations contain dark matter, gas and star particles with masses of  $1.11 \times 10^6 M_\odot$ ,  $2.2 \times 10^5 M_\odot$ , and  $< 6.3 \times 10^4 M_\odot$ , respectively, and a gravitational softening length of 310 pc. We analyze two *MaGICC* galaxies, *g1536* and *g15784*, which have been studied extensively previously (see Snaith et al. 2016, and references therein).

For both the *MaGICC* and *g14* simulations, halo membership is determined using the density-based halo finding algorithm AHF (Gill et al. 2004; Knollmann & Knebe 2009). We previously analyzed the *in situ* and accreted stellar halo from *g15784* in Valluri et al. (2016); in this work, any star belonging to the primary halo at present day is classified either as an *in situ* star or accreted star. Stars that are born in the primary halo are classified as *in situ* stars, while stars that are born in other bound structures are classified as accreted. Because we are interested in the kinematic properties of the stellar halo, we distinguish between *in situ* halo and *in situ* disk stars based purely on a spatial

<sup>8</sup> Our fiducial definition of a “dip” is a value of  $\beta$  that is at least 0.2 lower than  $\beta$  at the surrounding radii.

<sup>9</sup> found at <http://www.astro.columbia.edu/~kvj/halos/>



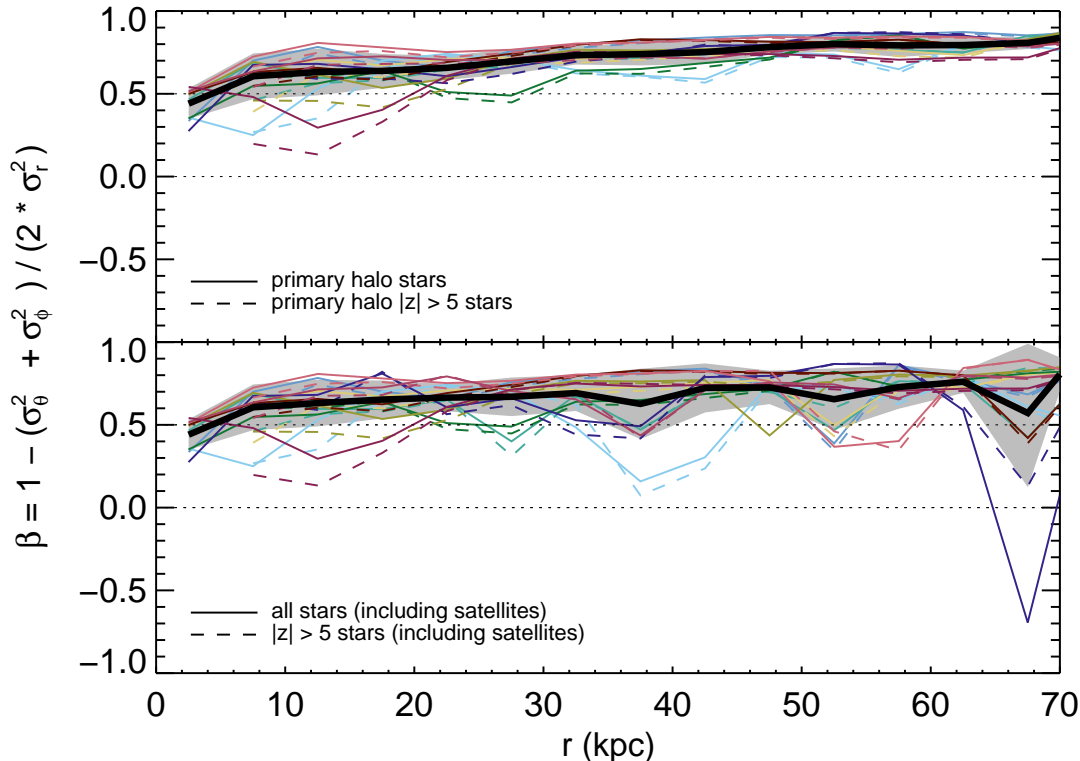


**Figure 1.**  $\beta$  as a function of radius for 11 stellar halos from BJ05. Top panel:  $\beta$  for stars belonging to primary halo at present day. Thin lines correspond to individual halos, thick line corresponds to average behavior, shaded gray shows area within  $1\sigma$  of the mean. Solid lines correspond to all stars and dashed lines correspond to  $|z| > 5$  kpc stars. Bottom panel:  $\beta$  for all stars within the virial radius (including satellites) at present day. The thin, thick, solid, and dashed lines and shaded region are the same as in the top panel.

cut; at present day, any *in situ* stars with  $|z| > 5$  kpc are considered *in situ* halo stars.<sup>10</sup> For *g1536*, 24% of the halo stars are *in situ* halo stars, and for the more massive system, *g15784*, 42% of the halo stars are *in situ* halo stars.

### 3. RESULTS

#### 3.1. Radially Anisotropic Trends

We begin by considering the  $z = 0$  behavior of  $\beta(r)$  for the BJ05 suite of simulations. As noted in §2.1, the BJ05 models are produced using a hybrid  $N$ -body + semi-analytic approach which results in stellar halos formed purely from accreted material. Henceforth, we adopt a fiducial radial bin size of 5 kpc.

The top panel of Figure 1 presents  $\beta(r)$  for the BJ05 models for stars that belong to the primary halo at present day. The behavior of each individual halo is shown by thin lines, while the average behavior of all 11 halos is shown in the thick black solid line surrounded by the  $1\sigma$  error bands shaded in gray. As a check, we look at  $\beta(r)$  for two cuts on the data: all the stars in the stellar halo (solid line), and just the stars with  $|z| > 5$  kpc (dashed line). There is no difference in the average  $\beta(r)$  values for these two populations. As also shown in Williams & Evans (2015) in the BJ05 suite the average trend is quite radially biased at all radii. From the small-

est radial bin outward,  $\beta \geq 0.5$ ; by  $r \sim 30$  kpc,  $\beta \sim 0.7$ , and for larger  $r$ ,  $\beta$  asymptotes to  $\sim 0.8$ . Regardless of merger history, all 11 halos show the same global behavior, trending toward large values of  $\beta$  at large  $r$ . In fact, the halo with a large late time accretion event (halo 9, shown in green) is relatively indistinguishable in  $\beta$  from the other 10 halos. While there are slight dips in  $\beta$  for individual halos, these dips never plummet to tangential or even isotropic values. Most dips are fairly small (on order 0.2 to 0.3 lower than the average  $\beta$  value), and beyond  $r \sim 20$  kpc, even these dips do not descend below  $\beta \sim 0.5$ .

The bottom panel of Figure 1 presents  $\beta(r)$  for all stars in the simulation, including those bound to infalling satellites. Because stars in a satellite lie within a small spatial volume and follow a coherent trajectory, including satellites generates dips in individual  $\beta(r)$  profiles; these dips are  $\sim 5 - 15$  kpc wide. A significant number of these dips fall below  $\beta \sim 0.5$ ; however, unexpectedly, very few of the dips could be considered isotropic and only one is tangential. Moreover, in the tangential instance (dark blue curve), it is very clear that the stars generating the dip belong to a small, coherent structure; this can be seen by the substantial difference in  $\beta$  for the full sample and the  $|z| > 5$  kpc sample at  $r \sim 65$  kpc.

We consider next the individual trends in the six  $N$ -body+SPH simulations from the *g14* and *MaGICC* suites. Here we select stars belonging to the stellar halo by a spatial cut ( $|z| > 5$  kpc). The top panel of Figure 2 shows  $\beta(r)$  for the stars that belong to the primary

<sup>10</sup> Throughout this work, we orient each simulated MW-like galaxy with its angular momentum vector pointed along the  $z$ -axis, ensuring its disk is aligned in the  $x$ - $y$  plane.

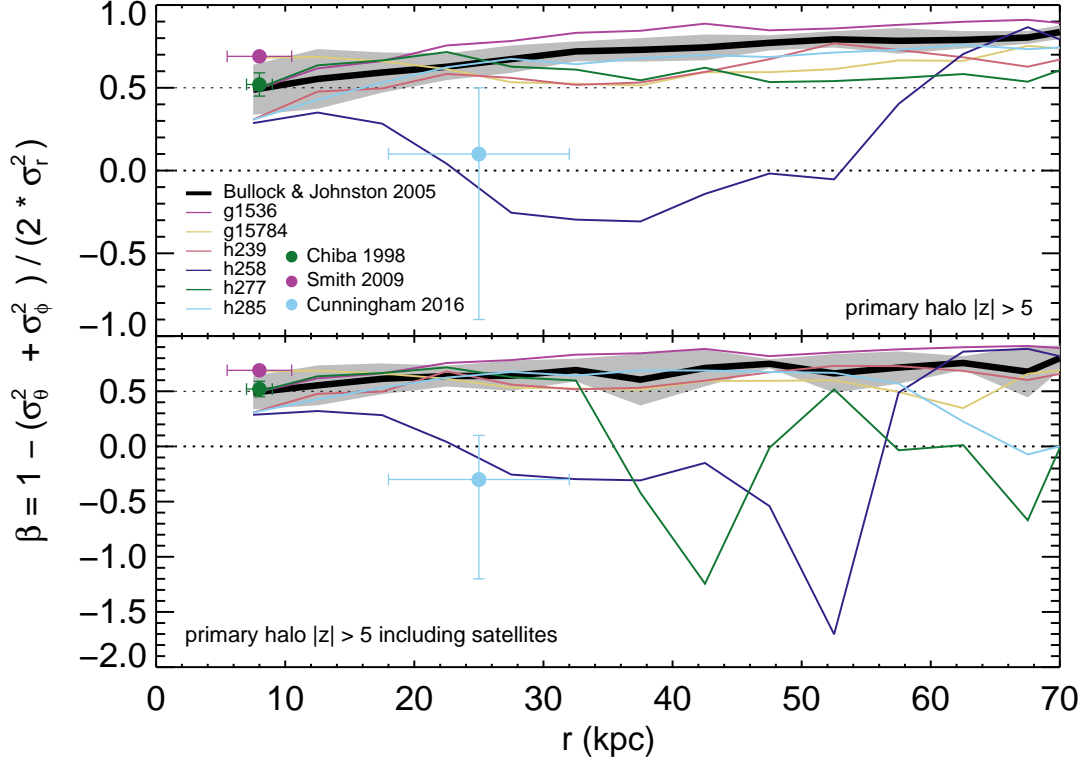


**Figure 2.** Top panel:  $\beta(r)$  profiles for all stars belonging to the primary stellar halos from 6 cosmological simulations (colored lines) and the average profile from BJ05 simulations (thick black curve), with the region within  $1\sigma$  of the mean for BJ05 shown in gray. Only one galaxy (*h258*) shows significant (negative) deviation from the average curve over a large range of radii (see §3.4 for details). The three points mark three measurements of  $\beta$  in the MW from 6D coordinates. Bottom panel: same as above for all stars including those bound to satellites within the virial radius at present day.

halo at the present day. Plotted in black is the average trend from Figure 1, with the  $1\sigma$  error band plotted in gray. Five of the six galaxies follow the BJ05 trend: from  $r \sim 10 - 15$  kpc onward,  $\beta \geq 0.5$ . For these galaxies,  $\beta$  never falls below 0.5 and generally trends toward larger values of  $\beta$  with increasing radius. While these five galaxies represent a wide range of merger histories for  $z < 1$ , their  $\beta(r)$  behavior is remarkably consistent with one another: *h239* (shown in salmon) has the most active merger history and yet its  $\beta(r)$  is virtually indistinguishable from *h277* (shown in green) which has a remarkably quiescent merger history until the very end of the simulation. Interestingly, the one galaxy that does not follow the BJ05 trend, *h258*, has a somewhat unremarkable merger history for  $z < 1$ . We will discuss this galaxy further in §3.2.3. It is remarkable, though, that none of the simulations' minor mergers from  $z < 1$  leave a lasting impression on  $\beta(r)$ .  $\beta$  is predicted by the average trends in BJ05, *g14*, and *MaGICC* suites to be  $\sim 0.5$  or larger at all radii at present day.

The three individual data points on Figure 2 mark existing measurements based on 6D data in the MW from nearby stars falling within  $\sim 2$  kpc from the Sun (Chiba & Yoshii 1998), SDSS stars in Stripe 82 with 5 kpc of the Sun (Smith et al. 2009), and from 13 HALO7D stars lying within  $18 < r/\text{kpc} < 32$  (Cunningham et al. 2016). Note that the measurements of anisotropy from nearby stars (green point) and SDSS (pink point) are completely consistent with predictions from all the sim-

ulations (except for *h258*). The error bars on the measurement from HALO7D (pale blue point) are large but the measured value, while still positive in the top panel, is significantly lower than the predictions from most of the simulations and intriguingly is consistent with the predictions from *h258*.

The bottom panel of Figure 2 presents  $\beta(r)$  for all stars in the simulation inside the virial radius of the primary halo but with  $|z| > 5$  kpc, including those bound to infalling satellites. Here, it is obvious that three of the six galaxies are interacting with satellites at present day: *h277*, *h285* and *g15784*. The first two of these galaxies have strongly tangential dips in  $\beta$ . These dips are much stronger than the tangential dip seen in BJ05. The dip in *g15784* ( $\beta \sim 0.4$ ) is still a radial value, but it would be stronger if the satellite was aligned differently with the disk, as it falls within  $|z| < 5$  kpc at the end of the simulation.

We conclude from this analysis of 17  $z = 0$  MW-like stellar halos that, except in the rarest of cases,  $\beta(r)$  is strongly predicted to be radially anisotropic beyond  $r \sim 8$  kpc. In fact, the average trends for all three suites of simulations predict that  $\beta \sim 0.5$  or larger at all radii at present day.

### 3.2. Deviations from Radial Anisotropy

As we have shown, a robust prediction of  $\Lambda$ CDM simulations is that stellar halos are radially anisotropic ( $\beta \geq 0.5$ ). However, recent analysis of 6D MW data

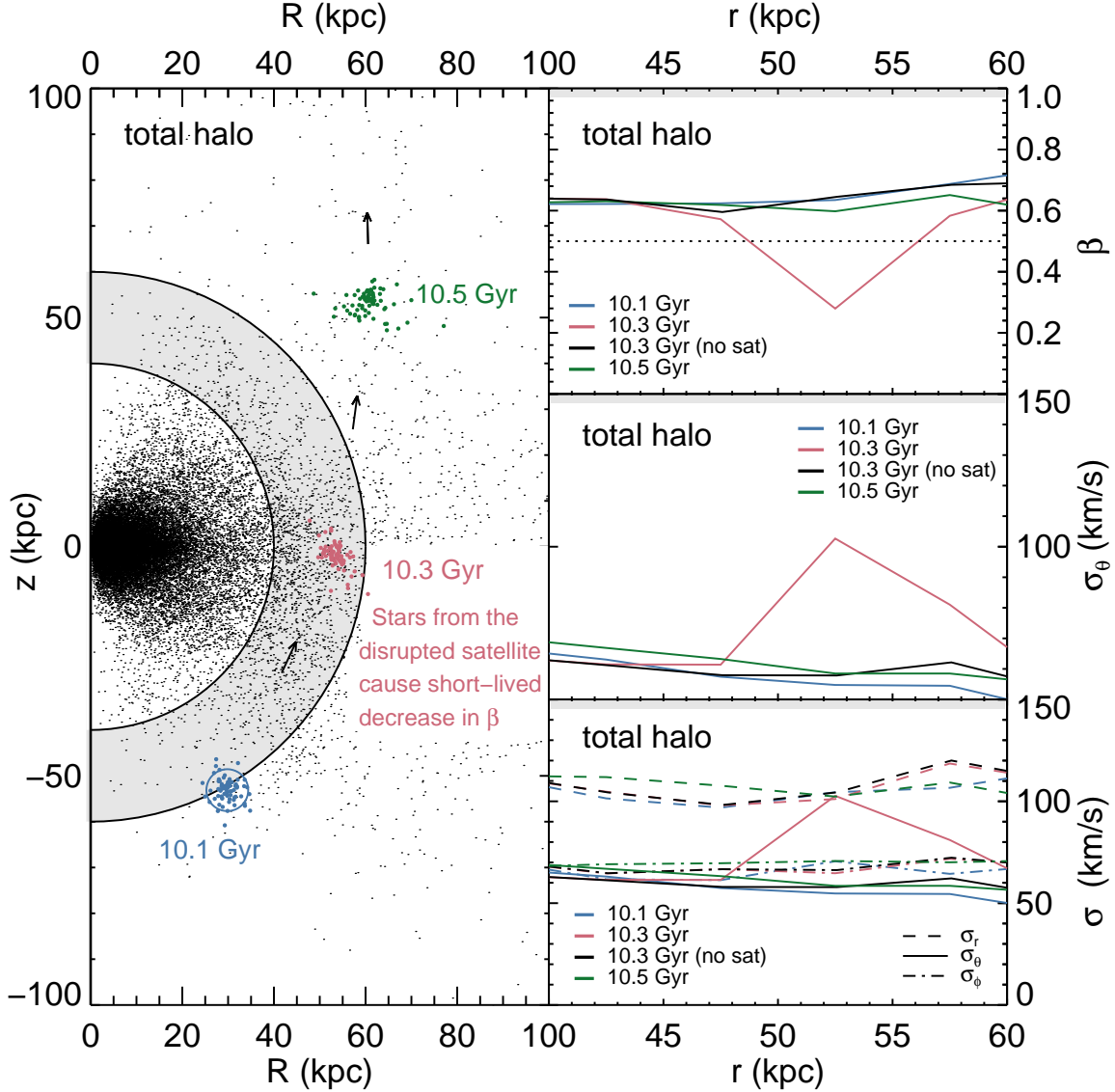


**Figure 3.** Illustration of the formation of a short-lived “dip” in  $\beta$  in the total (accreted+*in situ*) stellar halo of *g15784*. Left: The black points show the total stellar halo (in cylindrical coordinates) at 10.5 Gyr. The gray shaded region between the solid curves marks the radial shell for which  $\beta$  and  $\sigma$  profiles are shown in the other panels. Colored points mark the location of stars belonging to a disrupting satellite as it passes through the MW-like galaxy *g15784* at three different times (blue, red, dark green corresponding to time  $\sim 10.1$ , 10.3, and 10.5 Gyr); the circle on top of the stars at 10.1 Gyr indicates that the satellite is bound at this time. All of these stars are identified as belonging to *g15784*’s stellar halo by time  $\sim 10.3$  Gyr. The black arrows mark the trajectory of the stars as the satellite breaks up. Top right:  $\beta(r)$  profiles for total stellar halo at three different times (with and without the stars from the disrupted satellite at  $t = 10.3$  Gyr). Middle right: the corresponding polar velocity dispersion. Bottom right: all three components of the velocity dispersion for the total halo stars.

indicates a low value of  $\beta$  at larger radii in our galaxy (Cunningham et al. 2016); these observations prompt us to explore when and how rare departures from radial anisotropy occur in simulations. In what follows, we conduct a time series investigation of two hydrodynamic simulations, *g15784* from the *MaGICC* suite and *h258* from the *g14* suite; we explore three different scenarios when deviations from radial anisotropy occur:

1. An ongoing accretion event can cause a short-lived dip in  $\beta$  over a small range in radii.
2. Close passage of a large satellite galaxy can cause a longer-lived  $\beta$  dip in the *in situ* halo over a small range in radii.

3. A major merger event can cause a very long-lived tangential  $\beta$  feature across a large range of radii.

Here we illustrate each of these scenarios in turn.

### 3.2.1. Transient $\beta$ Dips in the Total Stellar Halo

We now consider the total stellar halo for *g15784*, which is dominated by accreted stars beyond  $r \sim 30$  kpc and is slightly oblate with a short/long axis ratio  $c/a \sim 0.85$ . At  $z = 0$ , *g15784* has a virial radius, virial mass, and stellar mass of  $R_{200} = 214$  kpc,  $M_{200} = 1.2 \times 10^{12} M_{\odot}$ , and  $M_{*} = 8.3 \times 10^{10} M_{\odot}$  respectively,<sup>11</sup> and experienced its last major merger at  $z$

<sup>11</sup> Here we have defined the virial radius to be  $R_{200}$ , the radius at which the average density of the halo is 200 times the critical

$\sim 1$ .

The left panel of Figure 3 illustrates the spatial distribution (in Galactocentric cylindrical coordinates,  $z$  versus  $R$ ) of stars in the stellar halo at time  $\sim 10.5$  Gyr (redshift  $z \sim 0.3$ ). The gray shaded region corresponds to a spherical shell spanning  $40 < r/\text{kpc} < 60$  containing a stellar halo mass of  $7.2 \times 10^7 M_\odot$ , which we look at in detail in the other three panels of Figure 3. At 10.1 Gyr, a bound satellite (stars shown in blue) enters the gray shaded region; this satellite contains a total stellar mass of  $2.6 \times 10^6 M_\odot$ . The black arrows show the direction of movement of the satellite. As it moves up through the mid-plane, the satellite is disrupted and no longer identified by the halo finding algorithm as a unique object. However, stars from this satellite maintain coherence for several time-steps, as illustrated by the location of these stars at 10.3 and 10.5 Gyr (shown in red and dark green in the top left panel of Figure 3).

The top right panel of Figure 3 shows  $\beta(r)$  for 10.1, 10.3 and 10.5 Gyr for stars falling within  $40 < r/\text{kpc} < 60$  and belonging to the total stellar halo at those time-steps. At 10.1 Gyr, the bound satellite enters the  $40 < r/\text{kpc} < 60$  shell. The  $\beta$  anisotropy at 10.1 Gyr is greater than 0.6 at all radii within the volume; at this time, the stars that belong to the satellite are not considered a part of stellar halo, and thus  $\beta(r)$  is not impacted by it. However, by 10.3 Gyr, the satellite has fully disrupted and stars from it are now considered a part of the total stellar halo; at this time a strong dip to  $\beta \sim 0.25$  appears at  $50 < r/\text{kpc} < 55$  (shown in red). This dip arises because stars from the disrupted satellite, which now lie inside this radial range, are on a polar orbit (as seen in the left panel) and hence their net orbital motion adds to the dispersion in the  $\theta$  direction. The former satellite's contribution can be seen clearly by contrasting  $\beta(r)$  for all the stars in the stellar halo (red line) to  $\beta(r)$  excluding the former satellite's stars (black line). The black line is greater than  $\sim 0.6$  at all radii, just like  $\beta(r)$  at 10.1 Gyr. At 10.5 Gyr,  $\beta(r)$  is no longer impacted by the former satellite in the range of radii under consideration, as the stars from the former satellite have moved out of the spherical shell.

Why does a dip form with the addition of the recently stripped stars? The middle right panel of Figure 3 shows  $\sigma_\theta$  at 10.1 (blue line), 10.3 (pink line), and 10.5 (dark green line) Gyr. Clearly,  $\sigma_\theta$  is substantially enhanced by adding the satellite stars; however,  $\sigma_\phi$ ,  $\sigma_r$  remain unchanged (see bottom right panel of Figure 3). This is because (as can be seen in the left panel) the satellite is on a predominantly polar orbit and hence the satellite debris has a large  $v_\theta$ . Again, when we remove stars from the disrupted satellite at 10.3 Gyr (black line) the dip in  $\sigma_\theta$  disappears, confirming that this coherent substructure is the source of the dip in  $\beta$ .

We track the disrupted satellite for several more time-steps and find the  $\beta$  dip does occur at larger radii, albeit to a lesser extent. This is because, as the disrupted satellite continues on its original orbit, it becomes increasingly radial. We note that this does not explain why the recently accreted stars do eventually turn radially anisotropic; however, the particulars of that transition are outside of the scope of this paper to explore.

density of the Universe, and the virial mass to be the total mass within the virial radius.

We conclude that dips in  $\beta$  generated in the total stellar halo are short-lived (lifetime  $< 0.2$  Gyr) and closely tied to recent accretion events. We suggest that hunting for such dips in velocity anisotropy, particularly at large radii, may be an effective means for identifying recently accreted but somewhat dispersed material.

### 3.2.2. $\beta$ Dips in the In Situ Stellar Halo

We now consider g15784's *in situ* stellar halo within  $25 < r/\text{kpc} < 45$  between 11.8 and 12.9 Gyr. As noted in §2.3, *in situ* halo stars are distinguished from *in situ* disk stars by a spatial cut at  $z = 0$ . At 11.8 Gyr, the number of *in situ* and accreted halo stars are roughly equal at 25 kpc, although the *in situ* stars are more concentrated toward the plane of the disk. Their kinematic behavior is also different; we see evidence of this in the response of the *in situ* stellar halo to the passage of a large, gas-rich satellite ( $M_{\text{total}} = 4.4 \times 10^{10} M_\odot$ ) through the volume at 12.3 Gyr.

The left panel of Figure 4 illustrates the spatial distribution (in Galactocentric cylindrical coordinates,  $z$  versus  $R$ ) of stars in the *in situ* stellar halo at time  $\sim 12.3$  Gyr. The gray shaded region corresponds to a spherical shell spanning  $25 < r/\text{kpc} < 45$  which we look at in detail in the other five panels of Figure 4. The unfilled circles show the location of the large satellite that passes through the volume at 11.8, 12.1, 12.3, 12.7 and 12.9 Gyr with black arrows indicating the direction of motion over time. At 12.3 Gyr, the satellite begins its passage through the region in question, but by 12.7 Gyr, the satellite has moved beyond the relevant volume. Note, no stars are donated by the satellite to the stellar halo during this passage, nor would such an exchange impact the *in situ* stellar halo, as *in situ* stars are by definition produced only in the primary halo.

The top right panel of Figure 4 shows  $\beta$  for all five moments in time for the *in situ* stars from the gray shaded region. Note, we require at least 20 star particles within each radial bin to calculate  $\beta$  and within  $30 < r/\text{kpc} < 35$  there are at least 125 *in situ* halo star particles at each time-step. Before the satellite interacts with g15784,  $\beta$  for the *in situ* stellar halo is consistent with the average behavior of BJ05; as can be seen by the dark and light blue lines for  $\beta$  at 11.8 and 12.1 Gyr respectively,  $\beta$  is either  $\sim 0.5$  or larger at all radii in question and is as high at  $\sim 0.7$  between  $30 < r/\text{kpc} < 35$  at 12.1 Gyr. However, starting at 12.3 Gyr onward,  $\beta$  sharply dips to  $0.2 - 0.3$  between  $30 < r/\text{kpc} < 35$ . This dip persists until the present day. Other such long lasting *in situ*  $\beta$  dips are found elsewhere in the *MaGICC* simulations and are coincident with the passage of a satellite through the  $z = 0$  plane; however, in all these other cases, the *in situ*  $\beta$  dips are radially anisotropic ( $\beta > 0$ ).

The kinematically hotter accreted stellar halo does not experience a similar dip in  $\beta$  at this radius at this epoch. Then why does the *in situ*  $\beta$  dip form and persist in this case? As can be seen in the second from the top panel on the right of Figure 4,  $\beta$  declined within  $30 < r/\text{kpc} < 35$  because  $\sigma_r$  decreases at 12.3 Gyr. However, as can be seen in the middle right panel of Figure 4, neither  $\sigma_\phi$  nor  $\sigma_\theta$  are appreciably altered. At the same time, it is clear that there is an increase in the mean streaming motion in this volume ( $\langle v_\phi \rangle$ ) (see the second from the bottom right panel of Figure 4). This increase appears to



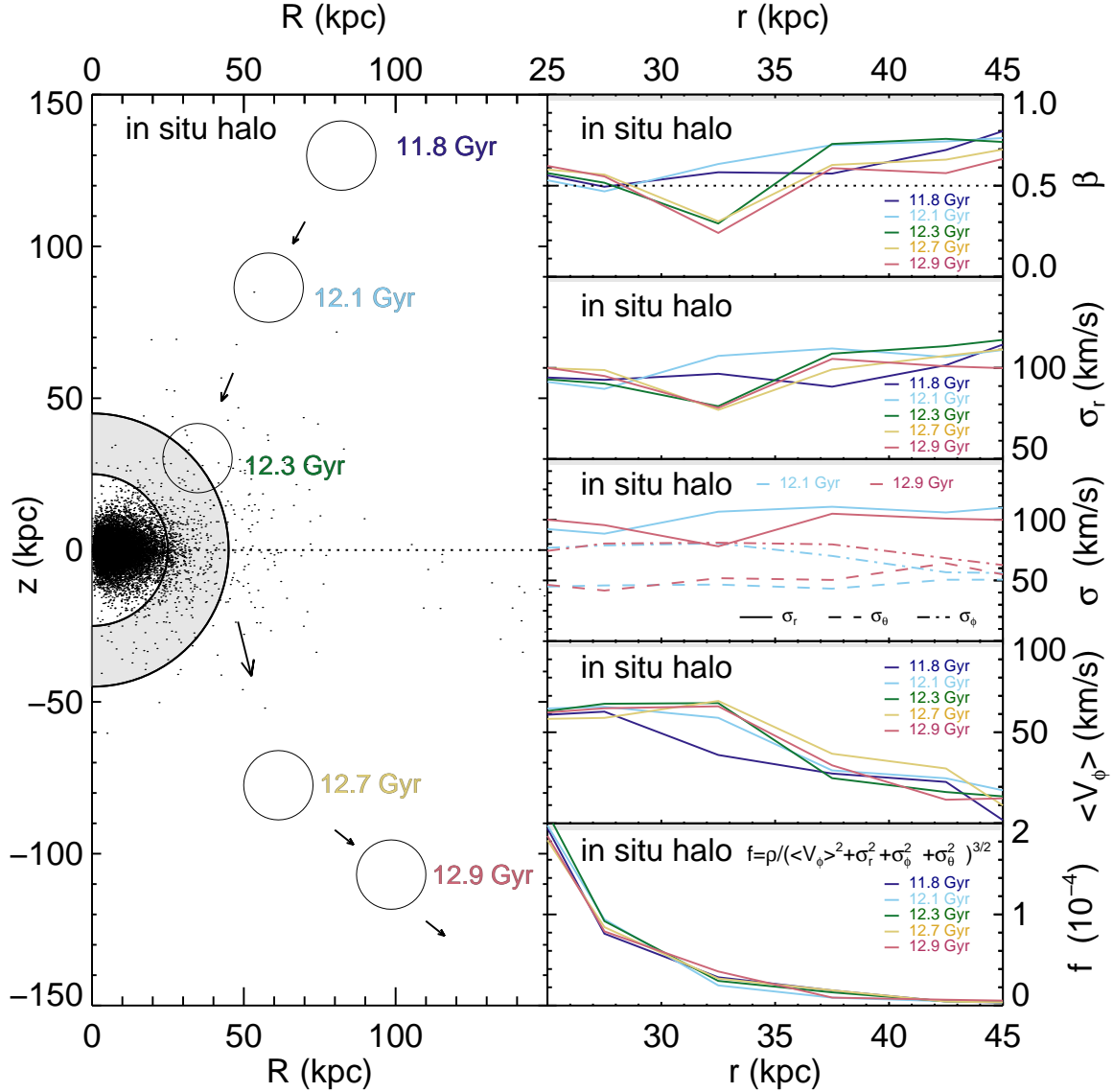


**Figure 4.** Illustration of the formation of a long-lived “dip” in  $\beta$  in the *in situ* stellar halo of *g15784*. Left: The black points show the *in situ* stellar halo (in cylindrical coordinates) at 12.3 Gyr. The gray shaded region between solid curves marks the radial shell for which  $\beta$  and  $\sigma$  profiles are shown in other panels. The open circles correspond to the position of a large  $M_{\text{total}} = 4.4 \times 10^{10} M_{\odot}$  satellite at five different times as indicated by the labels; black arrows mark the trajectory of the satellite. Top right:  $\beta(r)$  profiles for the *in situ* stellar halo at the five different times. Second from the top right: the corresponding radial velocity dispersion. Middle right: all three components of velocity dispersion for the *in situ* halo stars before and after the satellite interaction. Second from the bottom right: the corresponding mean azimuthal velocity profile at all five times. Bottom right: the (pseudo) coarse-grained phase-space density quantity,  $f = \rho / (\langle v_{\phi} \rangle^2 + \sigma_r^2 + \sigma_{\phi}^2 + \sigma_{\theta}^2)^{3/2}$  in units of  $10^{-4}$ . Note  $f$  is  $\sim$  constant with time, suggesting that this proxy for phase-space density is conserved.

result from torquing on the *in situ* halo stars originating from the passage of the massive satellite which imparts angular momentum to the *in situ* halo stars. During the encounter the satellite (which is moving retrograde relative to *g15784*’s disk’s rotation) loses orbital angular momentum. The increase in angular momentum of the *in situ* halo stars results in a corresponding decrease in  $\sigma_r$ . Note, we have computed the pseudo phase-space density,  $\rho / (\langle v_{\phi} \rangle^2 + \sigma_r^2 + \sigma_{\phi}^2 + \sigma_{\theta}^2)^{3/2}$ , for the *in situ* halo stars (bottom right panel of Figure 4), and it is clear that the radial profile of this quantity does not change during the interaction. This constancy in the coarse grained phase space density profile is reminiscent of the Liouville theorem although we caution that  $f$  is not the fine-grained

phase space density, to which the Liouville theorem applies. This suggests and the reason that the dip in  $\beta$  persists in this case is that the stars contributing to the dip have had their kinematic and density distributions permanently altered in a way that results in a long term equilibrium.

As noted in earlier studies, the *in situ* stellar halo is on average more metal-rich and has a lower  $\alpha$ -abundance than the accreted stellar halo (Zolotov et al. 2009; Tissera et al. 2013; Pillepich et al. 2015). In Valluri et al. (2016) and Loebman et al. (in prep), we analyze the ages, metallicity, and orbits of accreted and *in situ* stellar halos in the *MaGICC* suite, and we also find that the *in situ* halo stars are on average more metal-



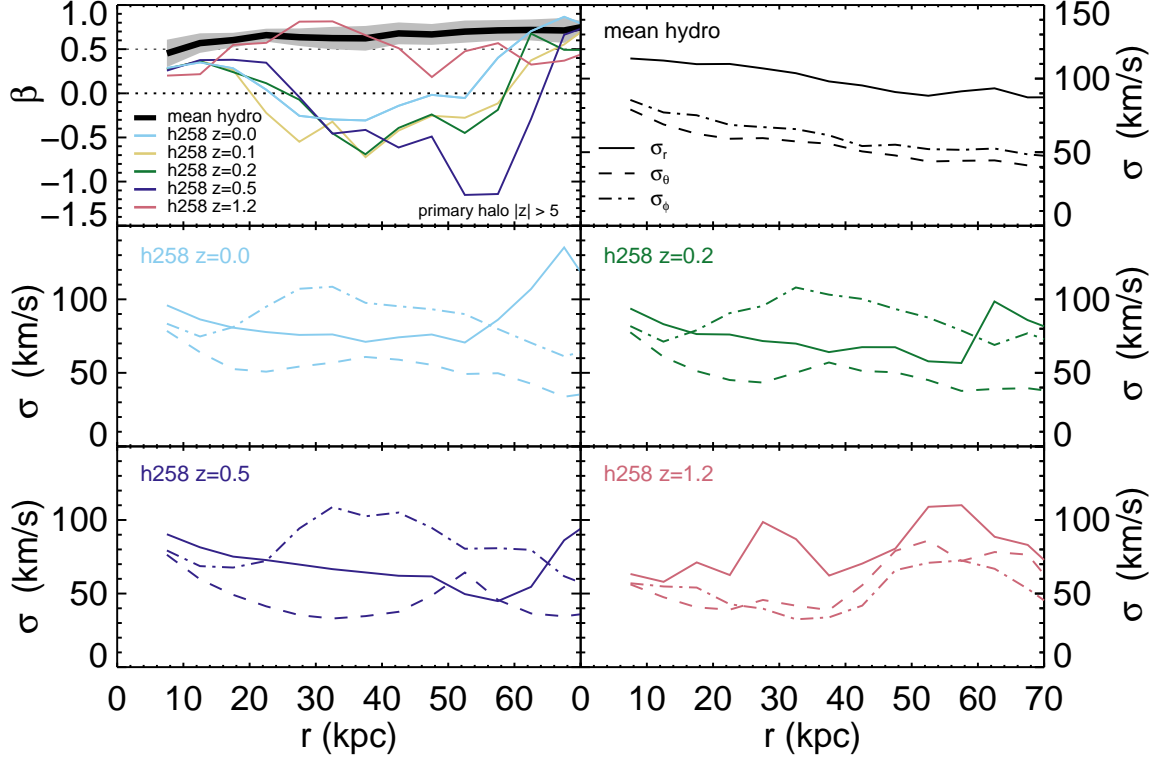


**Figure 5.** Signatures of major merger in *h258*. Top left:  $\beta(r)$  profiles at five different time-steps compared with the mean  $\beta(r)$  for the halo stars from the other five hydrodynamic simulations. The remaining panels show radial profiles of  $\sigma_r$ ,  $\sigma_\theta$  and  $\sigma_\phi$  for the mean of the 5 hydrodynamic simulations (top right) and for four other the time-steps. The middle panels and bottom left panel correspond to times after the merger event and the bottom right panel corresponds to a time before the merger event.

rich and have a lower  $\alpha$ -abundance than the accreted halo stars. While our detailed analysis of the connection between metallicity and *in situ* origin is forthcoming, we speculate that if  $\beta$  dips are identified in observational data-sets, then metallicity could be used to help distinguish between an *in situ* or accretion origin.

### 3.2.3. Merger Induced $\beta$ Trough

We consider now the  $\beta(r)$  outlier, *h258*, shown in dark blue in Figure 2. Like the other galaxies in the *g14* suite, *h258* is a good proxy for the MW at  $z = 0$  by total mass, total stellar mass, and bulge-to-disk ratio (Governato et al. 2009; Christensen et al. 2012); however, as discussed in Governato et al. (2009), *h258* experiences a major merger (mass ratio of merging halos 1.2 : 1) at  $z \sim 1$ . At this time, the progenitor galaxies plunge in on fairly radial orbits, with the internal spins of the two disks roughly aligned with the orbital angular momentum vector (see Figure 1a Governato et al. 2009). Over 1 Gyr, the progenitors experience two close passages, and finally coalesce at  $z \sim 0.8$ , thickening the stellar disks and populating the stellar halo in the process. From  $z \sim 0.8$  onward, the system has a relatively quiescent merger history as it regrows its thin disk through accreted gas.

In the top left panel of Figure 5, we consider  $\beta(r)$  over time for *h258*. Before the major merger occurs at  $z \sim 1.2$  (shown in pink),  $\beta(r)$  is consistent with the average profile for BJ05 for  $r < 30$  kpc. While  $\beta(r)$  does show a dip at  $r \sim 45$  kpc due to a satellite interaction, this dip

is minor (neither isotropic nor tangential).

However, for every time-step for  $z < 1$ ,  $\beta(r)$  shows a tangential to isotropic profile over a wide range of radii. That is, the imprint of  $z \sim 1$  merger event is encoded in the orbits of the halo stars. This can be seen clearly in the trends for each component of the velocity dispersion as a function of radius. The average trends for the five “normal” *N*-body+SPH galaxies from Figure 2 are shown in the top right hand panel of Figure 5; here at all radii  $\sigma_r > \sigma_\phi > \sigma_\theta$ . However, in the middle two panels and bottom left panel of Figure 5,  $\sigma_\phi > \sigma_r > \sigma_\theta$  over the radii in which  $\beta(r) \leq 0$ . This is due to a significant enhancement in  $\sigma_\phi$  and a minor cooling/suppression in growth of  $\sigma_r$ .

Physically, why does this happen? The nearly aligned merger of the two disk galaxies causes the disk stars to puff up into a rotating stellar halo with significant tangential velocity ( $v_\phi$ ). Simultaneously the near doubling in the total mass in the resultant galaxy deepens the potential well. This causes radial compression, decreasing the radial velocity dispersion of the halo stars in the process. Such baryonic compression without angular momentum transport causes orbits to become more tangentially biased (Quinlan et al. 1995; Debattista et al. 2008). Additionally,  $\sigma_r$  was small in both systems to begin with, owing to the disk stars having been in nearly circular orbits initially. And the near alignment of the galaxies maintains a net small  $\sigma_r$  after the merger.

While a merger event such as the one seen in *h258* may rarely occur, the kinematic record should be long

lasting, with  $\beta \leq 0$  over a wide range of radii at present day. Thus hunting for a broad  $\beta$  trough in the MW is of great value because it would give us deep insight into the MW’s major merger history.

#### 4. DISCUSSION AND CONCLUSIONS

The results and implications of this study are as follows:

1. Both accretion-only simulations and  $N$ -body+SPH simulations predict strongly radially anisotropic velocity dispersions in the stellar halos for most MW-like disk galaxies. The most robust observations in the Milky Way at  $r = 5 - 10$  kpc give  $\beta = 0.5 - 0.7$ , which is consistent with predictions from simulations.
2. There are three situations under which  $\beta$  “dips” or “troughs” (low positive to negative values of  $\beta$ ) arise in the simulations:
  - (a) Transient passage and disruption of a satellite which contributes a coherently moving group of stars to the stellar halo: such dips are short lived and last no longer than  $\sim 0.2$  Gyr.
  - (b) Passage of a massive satellite (that stays bound) through the inner part of the stellar halo induces transient changes in the kinematics of *in situ* halo stars. Such dips are longer lived, and because they affect the less dense but metal-rich *in situ* halo, they tend to be distinguishable by the fact that the stars contributing to the dip are metal-rich.
  - (c) A major merger with another disk at high redshift ( $z \sim 1$ ) can generate a stellar halo with a  $\beta$  trough – significant tangential anisotropy over a range of radii – which persists to the present day.

Previous results for  $\beta$  at  $r \sim 20 - 30$  kpc in the MW based on proper-motions (measured by *Hubble Space Telescope* in the direction of M31) suggest that  $\beta$  could be nearly zero or even slightly negative (Deason et al. 2013b; Cunningham et al. 2016). Such a low value of  $\beta$  could arise from substructure (as has been proposed by Deason et al. 2013b). If upcoming *Gaia* data confirms this dip in  $\beta$ , we predict that, if it was produced by recently disrupted satellite, then the  $\beta$  dip should be fairly localized in radius and unlikely to extend to all parts of the sky. If this dip is found to be to present primarily in high metallicity stars, it could point to the presence of an *in situ* stellar halo that was perturbed by the passage of a massive satellite. In the unlikely event that the dip is found over a large part of the sky and is highly negative over a wide range of radii, it could point to a major merger with a disk in the past.

It is clear that dips in  $\beta$  in the MW are a sensitive probe of recent interactions with satellites and long ago interactions with other disk galaxies. Determining proper-motions with *Gaia* and fully characterizing 6D phase-space with future surveys like WFIRST (Spergel et al. 2015) will enable us to explore substructure in the stellar halo in a new way. We posit that  $\beta$  should be thought

of as a tool for discovery, as it will enable us to find and follow-up on the building blocks of our stellar halo.

Finally, as mentioned in the introduction, one of the original motivations for determining the anisotropy parameter  $\beta$  is that this quantity appears in the spherical form of the Jeans equations (Jeans 1915) and knowledge of  $\beta(r)$  in the stellar halo would enable a determination of the mass profile of the MWs dark matter halo. However the assumption underlying the use of the spherical Jeans equation is that the tracer population and the potential that it traces are relaxed (virialized) and in dynamical equilibrium. As we have seen non-monotonic  $\beta$  profiles generally arise from substructure or perturbations which are clear evidence for a halo out of dynamical equilibrium. Since unvirialized systems tend to have higher kinetic energy than virialized systems the assumption of virial equilibrium would lead to an over-estimate in the halo mass. Furthermore for a given 3D velocity dispersion, an inferred tangential anisotropy also results in a higher estimate of the dynamical mass. This implies that if  $\beta$  in the MW stellar halo is found to be negative due to its non-equilibrium state, then dynamical measurements of the halo mass that use  $\beta$  are likely to overestimate the mass of the dark matter halo.

#### 5. ACKNOWLEDGMENTS

S.R.L. acknowledges support from the Michigan Society of Fellows. M.V. and K.H. are supported by NASA ATP award NNX15AK79G. V.P.D. is supported by STFC Consolidated grant ST/M000877/1. V.P.D. acknowledges being a part of the network supported by the COST Action TD1403 Big Data Era in Sky and Earth Observation. V.P.D. acknowledges the support of the Pauli Center for Theoretical Studies, which is supported by the Swiss National Science Foundation (SNF), the University of Zürich, and ETH Zürich and George Lake for arranging for his sabbatical visit during which time this paper was completed. V.P.D. acknowledges the Michigan Institute of Research in Astrophysics (MIRA), which funded his collaboration visit to the University of Michigan during which research for this paper was completed.

#### REFERENCES

- Abadi, M. G., Navarro, J. F., & Steinmetz, M. 2006, *MNRAS*, 365, 747
- Bell, E. F., et al. 2008, *Astroph. J.*, 680, 295
- Binney, J. 1980, *MNRAS*, 190, 873
- Binney, J., & Tremaine, S. 2008, *Galactic Dynamics: Second Edition* (Princeton University Press)
- Bird, S. A., & Flynn, C. 2015, *MNRAS*, 452, 2675
- Bond, N. A., et al. 2010, *Astroph. J.*, 716, 1
- Brooks, A. M., & Zolotov, A. 2014, *Astroph. J.*, 786, 87
- Bullock, J. S., & Johnston, K. V. 2005, *Astroph. J.*, 635, 931
- Chiba, M., & Yoshii, Y. 1998, *Astron. J.*, 115, 168
- Christensen, C., Quinn, T., Governato, F., Stilp, A., Shen, S., & Wadsley, J. 2012, *MNRAS*, 425, 3058
- Cunningham, E. C., Deason, A., Guhathakurta, P., Rockosi, C., Kirby, E., van der marel, r. p., & Sohn, S. T. 2015, *IAU General Assembly*, 22, 2255864
- Cunningham, E. C., et al. 2016, *Astroph. J.*, 820, 18
- Deason, A. J., Belokurov, V., Evans, N. W., & An, J. 2012, *MNRAS*, 424, L44
- Deason, A. J., Belokurov, V., Evans, N. W., & Johnston, K. V. 2013a, *Astroph. J.*, 763, 113
- Deason, A. J., Van der Marel, R. P., Guhathakurta, P., Sohn, S. T., & Brown, T. M. 2013b, *Astroph. J.*, 766, 24

- Debatista, V. P., Moore, B., Quinn, T., Kazantzidis, S., Maas, R., Mayer, L., Read, J., & Stadel, J. 2008, *Astroph. J.*, 681, 1076
- Diemand, J., Madau, P., & Moore, B. 2005, *MNRAS*, 364, 367
- Eggen, O. J., Lynden-Bell, D., & Sandage, A. R. 1962, *Astroph. J.*, 136, 748
- Font, A. S., Johnston, K. V., Bullock, J. S., & Robertson, B. E. 2006, *Astroph. J.*, 638, 585
- Gaia Collaboration, et al. 2016, *A&A*, 595, A1
- Gill, S. P. D., Knebe, A., & Gibson, B. K. 2004, *MNRAS*, 351, 399
- Gnedin, O. Y., Brown, W. R., Geller, M. J., & Kenyon, S. J. 2010, *ApJ*, 720, L108
- Governato, F., et al. 2009, *MNRAS*, 398, 312
- Governato, F., et al. 2012, *MNRAS*, 422, 1231
- Hattori, K., Yoshii, Y., Beers, T. C., Carollo, D., & Lee, Y. S. 2013, *ApJ*, 763, L17
- Jeans, J. H. 1915, *MNRAS*, 76, 70
- Johnston, K. V., Bullock, J. S., Sharma, S., Font, A., Robertson, B. E., & Leitner, S. N. 2008, *Astroph. J.*, 689, 936
- Kafle, P. R., Sharma, S., Lewis, G. F., & Bland-Hawthorn, J. 2012, *Astroph. J.*, 761, 98
- Katz, N., & White, S. D. M. 1993, *Astroph. J.*, 412, 455
- King, C., III, Brown, W. R., Geller, M. J., & Kenyon, S. J. 2015, *Astroph. J.*, 813, 89
- Knollmann, S. R., & Knebe, A. 2009, *Astroph. J. Suppl.*, 182, 608
- Munn, J. A., et al. 2004, *Astron. J.*, 127, 3034
- Munshi, F., et al. 2013, *Astroph. J.*, 766, 56
- Pillepich, A., Madau, P., & Mayer, L. 2015, *Astroph. J.*, 799, 184
- Quinlan, G. D., Hernquist, L., & Sigurdsson, S. 1995, *Astroph. J.*, 440, 554
- Rashkov, V., Pillepich, A., Deason, A. J., Madau, P., Rockosi, C. M., Guedes, J., & Mayer, L. 2013, *ApJ*, 773, L32
- Robertson, B., Bullock, J. S., Font, A. S., Johnston, K. V., & Hernquist, L. 2005, *Astroph. J.*, 632, 872
- Sales, L. V., Navarro, J. F., Abadi, M. G., & Steinmetz, M. 2007, *MNRAS*, 379, 1464
- Shen, S., Wadsley, J., & Stinson, G. 2010, *MNRAS*, 407, 1581
- Sirko, E., et al. 2004, *Astron. J.*, 127, 914
- Smith, M. C., et al. 2009, *MNRAS*, 399, 1223
- Snaith, O. N., Bailin, J., Gibson, B. K., Bell, E. F., Stinson, G., Valluri, M., Wadsley, J., & Couchman, H. 2016, *MNRAS*, 456, 3119
- Somerville, R. S., & Kolatt, T. S. 1999, *MNRAS*, 305, 1
- Spergel, D., et al. 2015, *ArXiv e-prints*
- Spergel, D. N., et al. 2003, *Astroph. J. Suppl.*, 148, 175
- Stinson, G., Brook, C., Maccio, A. V., Wadsley, J., Quinn, T. R., & Couchman, H. M. P. 2013, *Mon. Not. Roy. Astron. Soc.*, 428, 129
- Stinson, G., Seth, A., Katz, N., Wadsley, J., Governato, F., & Quinn, T. 2006, *MNRAS*, 373, 1074
- Tissera, P. B., Scannapieco, C., Beers, T. C., & Carollo, D. 2013, *MNRAS*, 432, 3391
- Valluri, M., Loebman, S. R., Bailin, J., Clarke, A., Debatista, V. P., & Stinson, G. 2016, in *IAU Symposium*, Vol. 317, *The General Assembly of Galaxy Halos: Structure, Origin and Evolution*, ed. A. Bragaglia, M. Arnaboldi, M. Rejkuba, & D. Romano, 358
- Wadsley, J. W., Stadel, J., & Quinn, T. 2004, *New Astronomy*, 9, 137
- Wang, W., Han, J., Cooper, A. P., Cole, S., Frenk, C., & Lowing, B. 2015, *MNRAS*, 453, 377
- Wilkinson, M. I., & Evans, N. W. 1999, *MNRAS*, 310, 645
- Williams, A. A., & Evans, N. W. 2015, *MNRAS*, 454, 698
- Xue, X.-X., et al. 2011, *Astroph. J.*, 738, 79
- Xue, X. X., et al. 2008, *Astroph. J.*, 684, 1143
- Zolotov, A., et al. 2012, *Astroph. J.*, 761, 71
- Zolotov, A., Willman, B., Brooks, A. M., Governato, F., Brook, C. B., Hogg, D. W., Quinn, T., & Stinson, G. 2009, *Astroph. J.*, 702, 1058